Mapping of Catalytic Residues in the RNA Polymerase Active Center

Article *in* Science · August 1996

DOI: 10.1126/science.273.5271.107 · Source: PubMed

10 authors, including:

Evgeny Zaychikov
Silantes GmbH
37 PUBLICATIONS **1,561** CITATIONS
SEE PROFILE

Emil Martin
University of Texas Medical School
85 PUBLICATIONS **3,949** CITATIONS
SEE PROFILE

Maxim Victorovich Kozlov
Russian Academy of Sciences
57 PUBLICATIONS **1,073** CITATIONS
SEE PROFILE

Vadim Markovtsov
Rigel
35 PUBLICATIONS **1,546** CITATIONS
SEE PROFILE

Mapping of Catalytic Residues in the RNA Polymerase Active Center

Evgeny Zaychikov, Emil Martin, Ludmila Denissova, Maxim Kozlov, Vadim Markovtsov, Mikhail Kashlev, Hermann Heumann, Vadim Nikiforov, Alex Goldfarb, Arkady Mustaev*

When the Mg^{2+} ion in the catalytic center of *Escherichia coli* RNA polymerase (RNAP) is replaced with Fe^{2+}, hydroxyl radicals are generated. In the promoter complex, such radicals cleave template DNA near the transcription start site, whereas the β′ subunit is cleaved at a conserved motif NADFDGD (Asn-Ala-Asp-Phe-Asp-Gly-Asp). Substitution of the three aspartate residues with alanine creates a dominant lethal mutation. The mutant RNAP is catalytically inactive but can bind promoters and form an open complex. The mutant fails to support Fe^{2+}-induced cleavage of DNA or protein. Thus, the NADFDGD motif is involved in chelation of the active center Mg^{2+}.

Magnesium ions play a crucial role in nucleic acid polymerization. In the single-subunit RNA and DNA polymerases that have been crystallized, Mg^{2+} chelated by acidic residues is directly involved in the catalytic reaction (*1*). By analogy, at least one of the three Mg^{2+} ions contained in the large multisubunit cellular RNAP (*2*) is likely to participate in catalysis. Residues that bind such catalytic Mg^{2+} should be among several evolutionarily conserved aspartates or glutamates in RNAP subunits.

To map the Mg^{2+}-binding site in *E. coli* RNAP, we used a combination of protein chemical and genetic approaches. Chelated Fe^{2+} generates highly reactive hydroxyl radicals, a technique used for DNA footprinting (*3*). We reasoned that the substitution of an Mg^{2+} for chelated Fe^{2+} in RNAP would cause a highly localized cleavage of nearby sites. Such cleavage was demonstrated previously for malic enzyme from pigeon liver (*4–6*), glutamine synthetase from *E. coli* (*7*), and the Tet repressor (*8*). To identify aspartates or glutamates that chelate Mg^{2+} in RNAP, we engineered a mutant carrying a triple alanine substitution of invariant Asp residues in the conserved region D of the β′ subunit (Fig. 1). The mutant DDD RNAP was reconstituted from individually expressed subunits (*9*) and compared with the wild-type enzyme in the Fe^{2+}-induced localized cleavage reaction.

The addition of Fe^{2+} to the wild-type RNAP-T7A1 promoter complex produced a strong cleavage of the DNA template strand at positions −1 and −2 relative to the transcription start site (Fig. 2, lane 3). The reaction is inhibited by Mg^{2+}. The requirement of dithiothreitol (DTT) (Fig. 2, lane 4) indicates that the cleavage is not hydrolytic but is induced by hydroxyl radicals (*10*). Under these conditions, hydroxyl radicals are generated from soluble O_2 in a catalytic fashion (*3*, *10*).

The DDD mutant RNAP failed to cleave DNA (Fig. 2, lanes 5 through 7). Nevertheless, the DDD RNAP formed the open promoter complex, as revealed by permanganate footprinting of the transcription bubble (Fig. 3). The ability of the DDD polymerase to form a stable open promoter complex was confirmed by deoxyribonuclease (DNase) I footprinting and DNA bandshift analysis. Yet the mutant was totally inactive in polymerization and abortive initiation assays in vitro. In vivo, the mutation was a dominant lethal, presumably because the DDD enzyme bound to promoters and made them inaccessible to the wild-type polymerase.

We asked whether the replacement of the Mg^{2+} ion in RNAP with Fe^{2+} would cause cleavage of RNAP protein. To this end, RNAP exposed to Fe^{2+} was fractionated by SDS–polyacrylamide gel electrophoresis (SDS-PAGE) and stained with Coomassie blue. Two identical experiments are shown that represent a longer (Fig. 4A) or shorter (Fig. 4B) electrophoresis run to permit better separation of the large subunits and visualization of the short cleavage

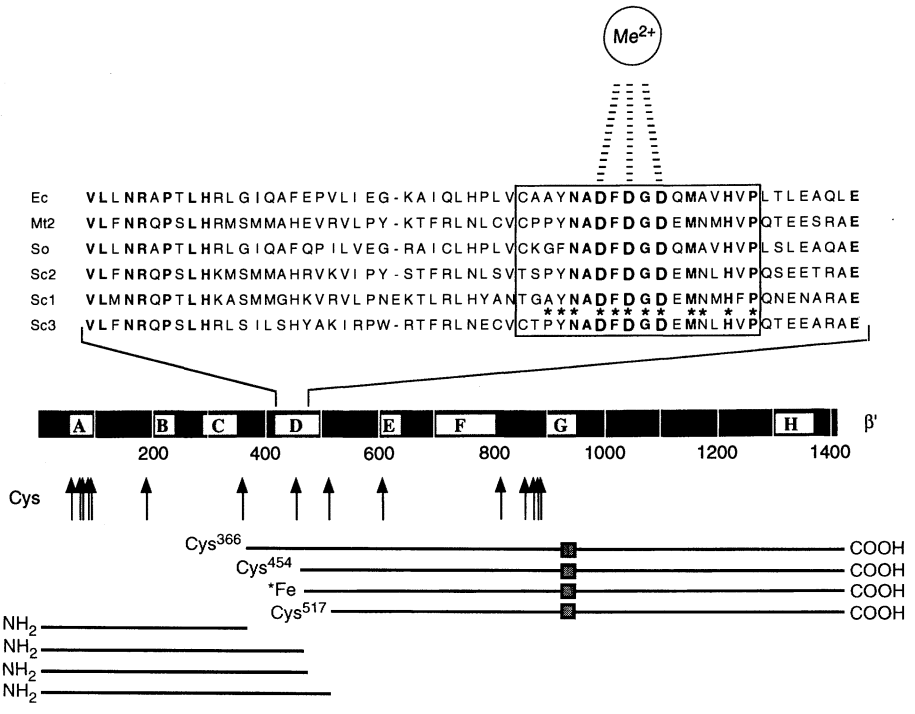

Fig. 1. Metal-binding aspartates in the β′ subunit (*13*). A scheme of the 1407–amino acid β′ polypeptide is represented by a horizontal bar with conserved regions shown as lettered boxes. Sequence alignments in the D region are as follows. Ec, *E. coli*; Mt2, *Methanobacterium thermoautotrophicum*; So, *Spinacia oleracea chloroplast*; Sc1, *Saccharomyces cerevisiae* Pol I; Sc2, *S. cerevisiae* Pol II; Sc3, *S. cerevisiae* Pol III. The conserved region D containing the NADFDGD motif is boxed. Asterisks indicate the positions of lethal single-site substitutions obtained by Dieci *et al.* (*18*). The putative Me^{2+}-binding site is highlighted. The bottom part of the figure presents the scheme of mapping of the major Fe^{2+} cleavage site. Positions of Cys residues are shown by arrows. The principal single-hit Cys marker fragments are shown underneath. The Rif-G**p**Cp*T* tag (see text) is represented by dark gray boxes.

E. Zaychikov and L. Denissova, Limnological Institute, Russian Academy of Sciences, Irkutsk 664033, Russia. E. Martin, M. Kozlov, V. Markovtsov, M. Kashlev, V. Nikiforov, A. Goldfarb, A. Mustaev, Public Health Research Institute, 455 First Avenue, New York, NY 10016, USA. H. Heumann, Max-Planck-Institut fur Biochemie, 8033 Martinsreid bei Munchen D82152, Germany.

*To whom correspondence should be addressed.

products, respectively. Fe^{2+} caused substantial degradation of the wild-type but not of the mutant enzyme. The β′ subunit was cleaved predominantly and was also cleaved preferentially at a single site producing two principal products of approximately 100 and 50 kD. The β subunit was degraded to a lesser extent.

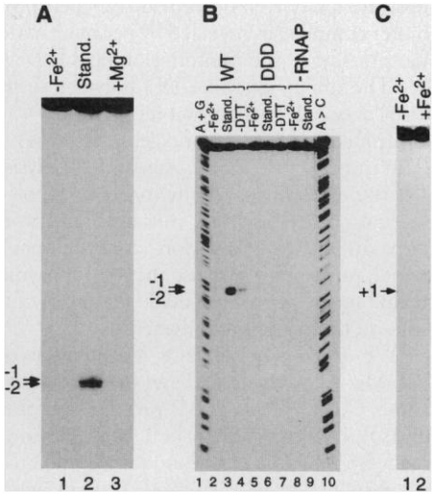

Fig. 2. Fe^{2+} cleavage of DNA in the RNAP-promoter complex. In the standard reaction (Stand.) (lanes 2 and 3), the wild-type or *DDD* mutant RNAP (1.6 μg) was incubated with 0.3 μg of the T7A1 promoter DNA fragment labeled at either the template strand (**A** and **B**) or the nontemplate strand (**C**) in 10 μl of BB buffer [8 mM Hepes (pH 8), 50 mM NaCl, 6 mM $MgCl_2$, and 1 mM DTT] for 5 min at 37°C and then dialyzed against 8 mM Hepes and 1 mM DTT on a VS membrane (Millipore) for 2 hours at room temperature. The complex was then treated for 5 min at 37°C with 20 μM $Fe(NH_4)_2(SO_4)_2$. The DNA was then precipitated with ethanol, dissolved in 80% formamide, and analyzed on a 7% sequencing gel. Where indicated, Fe^{2+} or DTT was omitted from the standard reaction or Mg^{2+} was added. A + G and A > G are sequence ladders. The DDD mutant RNAP was reconstituted from individually expressed subunits (*9*). The mutation was engineered as described (*24*). A + G is the sequencing ladder used as reference.

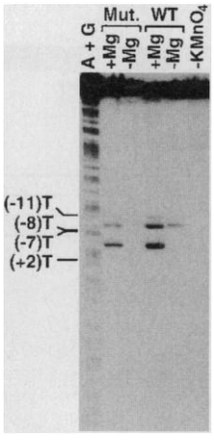

Fig. 3. Open promoter complex formation by the wild-type (WT) and DDD mutant (Mut.) RNAP. Complexes between RNAP and the T7A1 promoter DNA fragment labeled at the nontemplate strand (*25*) were dialyzed against 8 mM Hepes and 1 mM DTT either containing or missing $MgCl_2$ (6 mM) as indicated, and then treated with 1 mM $KMnO_4$ for 2 min at 37°C. After ethanol precipitation and exposure to piperidine (20 min at 90°C), the nucleotide material was resolved in 7% sequencing gel and radioautographed. A + G is the sequencing ladder used as reference. Numbers at left indicate positions of thymidine residues susceptible to $KMnO_4$.

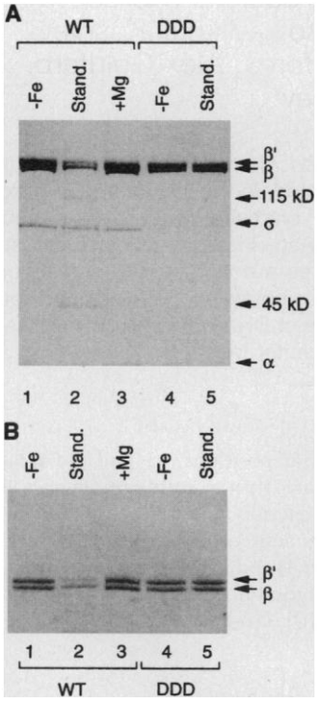

Fig. 4. Fe^{2+} induced cleavage of RNAP. The RNAP-promoter complex was formed with unlabeled DNA, treated with Fe^{2+} as described in the legend to Fig. 2, and analyzed in a denaturing 10% SDS gel that was stained with Coomassie blue. The gel in (**B**) is the same as that in (**A**) but was run two times longer in order to resolve the β and β′ subunits.

Our attempts to directly sequence the NH_2-terminus of the major cleavage site were unsuccessful, either because the terminus was modified or as a result of multiple cleavages. To map the cleavage site indirectly, the wild-type β′ subunit was labeled by a radioactive affinity tag. In the affinity-labeling protocol, initiation on a promoter is primed with a Rifampicin-nucleotide compound (*11*) [Rif–guanosine triphosphate (GTP)] in combination with [α-^{32}P]CTP (the second nucleotide) and a derivative of TTP (the third nucleotide) with an alkylating group in the 3′ position of ribose. In this reaction, RNAP becomes specifically tagged with Rif-G**p**C*p*T (bold indicates radioactive phosphate and italics indicate the cross-linked nucleotide) at Met^{932} of the β′ subunit (*12*). The radiotagged ternary complex was subjected to Fe^{2+}-mediated cleavage and the products were separated by SDS-PAGE and visualized by autoradiography (Fig. 5). As markers for the cleavage site mapping, we used fragments of the same β′ subunit generated by single-hit degradation with 2-nitro-5-thiocyanobenzoic acid (NTCBA) and cyanogen bromide (CNBr), which cleave proteins at Cys and Met residues, respectively.

The 100-kD fragment is clearly the major product of the Fe^{2+} cleavage reaction (Fig. 5, lane 2). To obtain two levels of fragment resolution, shorter (Fig. 5, lanes 1 through 4) and longer (Fig. 5, lanes 5 through 7) electrophoretic runs were performed. From

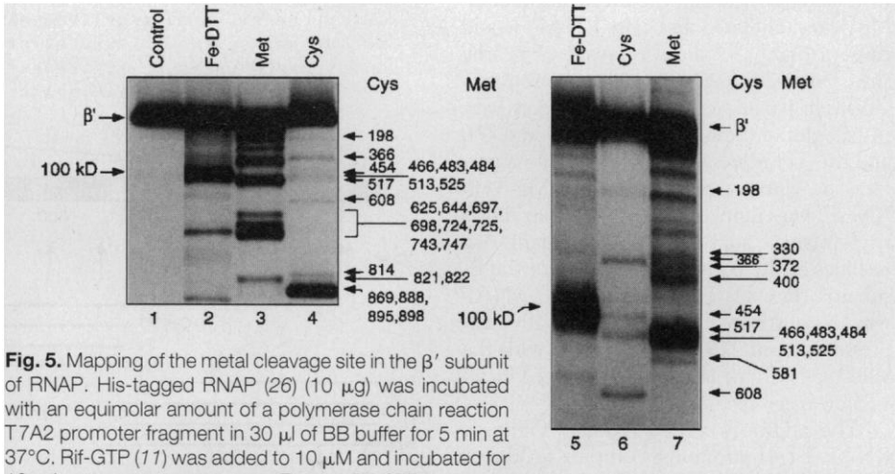

Fig. 5. Mapping of the metal cleavage site in the β′ subunit of RNAP. His-tagged RNAP (*26*) (10 μg) was incubated with an equimolar amount of a polymerase chain reaction T7A2 promoter fragment in 30 μl of BB buffer for 5 min at 37°C. Rif-GTP (*11*) was added to 10 μM and incubated for 10 min at room temperature. Excess Rif-GTP was removed by adsorption of the complex on Ni-nitrilotriacetic acid agarose beads and washing with 1 ml of BB buffer (*27*). [α-^{32}P]CTP (0.3 μM) was added for 10 min, the complexes were washed three times with BB buffer containing 2.5 mM $MnCl_2$ instead of $MgCl_2$, and the mixture was supplemented with 3′-deoxy-3′-bromacetamido–thymidine triphosphate (*12*) to final concentration of 100 μM. After 30 min at 37°C, the beads were washed with 10 mM Hepes (pH 8) and 50 mM NaCl, and Fe^{2+} cleavage (lanes 2 and 5) was performed as described above. The protein was eluted from the resin with 50 μl of a buffer containing 100 mM imidazole, 10% glycerol, 1% DTT, and 1% SDS, and analyzed by SDS-PAGE. The control lane shows the uncleaved material eluted from the beads. Limited CNBr and NTCBA cleavages were performed as previously described (*19*). Arrows mark the positions of Cys and Met residues in the sequence ladders.

the Met markers pattern, the major Fe^{2+} cleavage occurs between Met^{466} and Met^{400} (Fig. 5, lane 7). At the same time, the major cleavage product co-migrates with the Cys^{454} marker (Fig. 5, lane 6; and Fig. 1). As can be seen from Fig. 1, Cys^{454} flanks the evolutionarily conserved region D of the β′ polypeptide containing the NADFDGD (*13*) sequence. Thus, the major Fe^{2+} cleavage occurs next to this motif.

These results strongly suggest that the aspartates of the NADFDGD sequence are involved in chelating the Mg^{2+} ion in the active center of RNAP (*14*). In DNA polymerase I and human immunodeficiency virus reverse transcriptase, the acidic residues that perform this function are located at the base of the cleft in the three-dimensional (3D) structure, the site where the catalytic reaction is believed to take place (*1*). A similar cleft has been observed in low-resolution contours of RNAP from *E. coli* (*15*) and yeast RNAP II (*16*) and RNAP I (*17*). Thus, in these large multisubunit RNAPs, the NADFDGD motif is probably located in the base of the cleft, where it forms the crucial element of the active center. Further evidence for the functional importance of the NADFDGD motif has come from extensive mutagenesis performed on yeast RNA polymerase III (*18*). Previous cross-linking experiments have implicated other sites in the active center of *E. coli* RNAP. Segments 515 to 660 and 1091 to 1107 in β and 330 to 366 and 932 to 1020 in β′ are facing the 3′ terminus of RNA in the catalytic pocket (*19*, *20*). Lys^{1065} and His^{1237} of the β subunit are located on the 5′ side facing the priming nucleoside triphosphate (*21*, *22*). The Rif-binding site is located upstream of the 5′ face along the exit path of the transcript (*12*, *23*). Our present results indicate that all these sites are juxtaposed to the NADFDGD motif in the 3D structure of RNAP and probably line the surface of the cleft where the active center is located.

REFERENCES AND NOTES

1. C. M. Joyce and T. A. Steitz, *Annu. Rev. Biochem.* **63**, 777 (1994).
2. W.-C. Suh, S. Leirmo, T. Record Jr., *Biochemistry* **31**, 7815 (1992).
3. M. A. Price and T. D. Tullius, *Methods Enzymol.* **212**, 194 (1992).
4. C. H. Wei, W. Y. Chou, S. M. Huang, C. C. Lin, G. G. Chang, *Biochemistry* **33**, 7931 (1994).
5. C. H. Wei, W. Y. Chou, G. G. Chang, *ibid.* **34**, 7949 (1995).
6. W. Y. Chou, W. P. Tsai, C. C. Lin, G. G. Chang, *J. Biol. Chem.* **270**, 25935 (1995).
7. J. M. Farber and R. L. Levine, *ibid.* **261**, 4574 (1986).
8. N. Ettner *et al.*, *Biochemistry* **34**, 22 (1995).
9. S. Borukhov and A. Goldfarb, *Protein Expr. Purif.* **4**, 503 (1993).
10. D. G. Knorre, O. S. Fedorova, E. I. Frolova, *Russ. Chem. Rev.* **62**, 65 (1993).
11. A. A. Mustaev *et al.*, *Proc. Natl. Acad. Sci. U.S.A.* **91**, 12036 (1994).
12. V. Markovtsov, in preparation.
13. Abbreviations for the amino acid residues are as follows: A, Ala; C, Cys; D, Asp; E, Glu; F, Phe; G, Gly; H, His; I, Ile; K, Lys; L, Leu; M, Met; N, Asn; P, Pro; Q, Gln; R, Arg; S, Ser; T, Thr; V, Val; W, Trp; and Y, Tyr.
14. Mg^{2+} is also required for promoter opening [W.-C. Suh, W. Ross, T. Record Jr., *Science* **259**, 358 (1993)]. Because the DDD mutant opens the promoter, the Mg^{2+} ion involved in the opening must be different from the one held by the substituted aspartates in the active center.
15. S. A. Darst, E. W. Kubalek, R. D. Kornberg, *Nature* **340**, 730 (1989).
16. S. A. Darst, A. M. Edwards, E. W. Kubalek, R. D. Kornberg, *Cell* **66**, 121 (1991).
17. P. Schultz, H. Celia, M. Riva, A. Sentenac, P. Oudet, *EMBO J.* **12**, 2607 (1993).
18. G. Dieci *et al.*, *ibid.* **14**, 3766 (1995).
19. V. Markovtsov, A. Mustaev, A. Goldfarb, *Proc. Natl. Acad. Sci. U.S.A.* **93**, 3221 (1996).
20. S. Borukhov, J. Lee, A. Goldfarb, *J. Biol. Chem.* **266**, 23932 (1991).
21. M. A. Grachev *et al.*, *Eur. J. Biochem.* **180**, 577 (1989).
22. A. Mustaev *et al.*, *J. Biol. Chem.* **266**, 23927 (1991).
23. K. Severinov *et al.*, *ibid.* **270**, 29428 (1995).
24. E. Martin, thesis, Institute of Molecular Genetics, Russian Academy of Science, Moscow (1992).
25. E. Zaychikov, L. Denissova, H. Heumann, *Proc. Natl. Acad. Sci. U.S.A.* **92**, 1739 (1994).
26. M. Kashlev, *et al.*, *Gene* **130**, 9 (1993).
27. E. Nudler, A. Goldfarb, M. Kashlev, *Science* **265**, 793 (1994).

28. Supported by a grant from NIH (to A.G.), by a grant from Deutsche Forschung-Gemeinschaft (to H.H.), and by a Fogarty International Research Collaboration Award grant (to A.G. and E.Z.). We are grateful to S. Borukhov and E. Nudler for comments.

20 February 1996; accepted 17 April 1996

Prevention of Islet Allograft Rejection with Engineered Myoblasts Expressing FasL in Mice

Henry T. Lau,* Ming Yu, Adriano Fontana, Christian J. Stoeckert Jr.

Allogeneic transplantation of islets of Langerhans was facilitated by the cotransplantation of syngeneic myoblasts genetically engineered to express the Fas ligand (FasL). Composite grafting of allogeneic islets with syngeneic myoblasts expressing FasL protected the islet graft from immune rejection and maintained normoglycemia for more than 80 days in mice with streptozotocin-induced diabetes. Graft survival was not prolonged with composite grafts of unmodified myoblasts or Fas-expressing myoblasts. Islet allografts transplanted separately from FasL-expressing myoblasts into the contralateral kidney were rejected, as were similarly transplanted third-party thyroid allografts. Thus, the FasL signal provided site- and immune-specific protection of islet allografts.

Immunological rejection of pancreatic islet allografts remains a major obstacle toward the application of such transplants in the treatment of diabetes mellitus. Interactions of Fas with its ligand (FasL) are thought to play a major role in the maintenance of immunological homeostasis and peripheral tolerance (*1*). We investigated whether provision of the FasL signal by transfected syngeneic myoblasts within the local environment of an islet allograft can deliver a death signal to infiltrating allo-activated T cells that express Fas (*2*) and thereby protect the islet allograft from rejection. This approach could permit the use of plasmid-based gene delivery into carrier cells such as myoblasts and make unnecessary the direct transfection of islet allografts.

A muscle cell–based delivery system that is effective in the delivery of recombinant molecules (*3*) was used. Primary myoblasts from adult C57BL/6 (B6) ($H\text{-}2^b$) mice were transfected with the plasmid BCMGS Neo-FasL (*4*), and G418-resistant colonies were pooled and designated Bfasl. These cells were analyzed for FasL expression by fluorescence-activated cell sorting (FACS) with the fusion protein Fas-Fc, which is the specific counterreceptor for FasL. The Bfasl cells were positive for FasL, whereas non-transfected B6 myoblasts (designated B6a) showed only background staining (Fig. 1A). The ability of B6 myoblasts to express recombinant FasL and to survive is consistent with the observation that muscle cells do not express Fas (*5*). The Fas^+ murine lymphoma cell line YAC-1 was used as a target in a cytotoxicity assay (*6*) to ascertain whether the FasL-expressing myoblasts could deliver an apoptotic signal to Fas-bearing cells. Bfasl myoblasts cocultured with YAC-1 cells for 12 hours induced YAC-1 cell death (Fig. 1B) and DNA fragmentation (Fig. 1C), consistent with death by apoptosis (*7*), whereas coculture with

H. T. Lau and M. Yu, Department of Pediatric Surgery, Children's Hospital of Philadelphia, University of Pennsylvania, Philadelphia, PA 19104, USA
A. Fontana, Department of Internal Medicine, Section of Clinical Immunology, University Hospital of Zurich, Haldeliweg 4, CH-8044 Zurich, Switzerland.
C. J. Stoeckert Jr., Department of Hematology, Abramson Center, Children's Hospital of Philadelphia, Philadelphia, PA 19104, USA.

*To whom correspondence should be addressed at Department of Pediatric Surgery, Johns Hopkins Hospital, Baltimore, MD 21287, USA.

References and Notes

[11] **Topology of the RNA Polymerase Active Center Probed by Chimeric Rifampicin-Nucleotide Compounds**

Arkady Mustaev; Evgeny Zaychikov; Konstatin Severinov; Mikhail Kashlev; Andrey Polyakov; Vadim Nikiforov; Alex Goldfarb

Proceedings of the National Academy of Sciences of the United States of America, Vol. 91, No. 25. (Dec. 6, 1994), pp. 12036-12040.

Stable URL:

http://links.jstor.org/sici?sici=0027-8424%2819941206%2991%3A25%3C12036%3ATOTRPA%3E2.0.CO%3B2-O

[14] **Two Open Complexes and a Requirement for Mg 2+ to Open the #PR Transcription Start Site**

Won-Chul Suh; Wilma Ross; M. Thomas Record, Jr.

Science, New Series, Vol. 259, No. 5093. (Jan. 15, 1993), pp. 358-361.

Stable URL:

http://links.jstor.org/sici?sici=0036-8075%2819930115%293%3A259%3A5093%3C358%3ATOCAAR%3E2.0.CO%3B2-L

[19] **Protein-RNA Interactions in the Active Center of Transcription Elongation Complex**

Vadim Markovtsov; Arkady Mustaev; Alex Goldfarb

Proceedings of the National Academy of Sciences of the United States of America, Vol. 93, No. 8. (Apr. 16, 1996), pp. 3221-3226.

Stable URL:

http://links.jstor.org/sici?sici=0027-8424%2819960416%2993%3A8%3C3221%3APIITAC%3E2.0.CO%3B2-2

LINKED CITATIONS

[27] **Discontinuous Mechanisms of Transcription Elongation**

Evgeny Nudler; Alex Goldfarb; Mikhail Kashlev

Science, New Series, Vol. 265, No. 5173. (Aug. 5, 1994), pp. 793-796.

Stable URL:

http://links.jstor.org/sici?sici=0036-8075%2819940805%293%3A265%3A5173%3C793%3ADMOTE%3E2.0.CO%3B2-4